IEEE Photonics Journal
An IEEE Photonics Society Publication

Open Access

Fluorescence Signal Generation Optimization by Optimal Filling of the High Numerical Aperture Objective Lens for High-Order Deep-Tissue Multiphoton Fluorescence Microscopy

Volume 7, Number 6, December 2015

Ke Wang
Runfu Liang
Ping Qiu

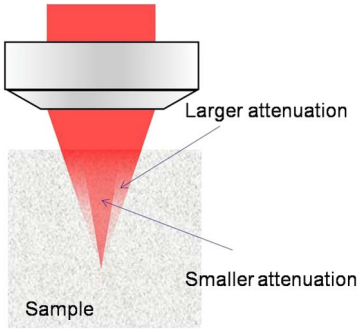

DOI: 10.1109/JPHOT.2015.2505145
1943-0655 © IEEE

Fluorescence Signal Generation Optimization by Optimal Filling of the High Numerical Aperture Objective Lens for High-Order Deep-Tissue Multiphoton Fluorescence Microscopy

Ke Wang,[1] Runfu Liang,[1] and Ping Qiu[2]

[1]Key Laboratory of Optoelectronic Devices and Systems of Ministry of Education and Guangdong Province, College of Optoelectronic Engineering, Shenzhen University, Shenzhen 518060, China
[2]College of Physics Science and Technology, Shenzhen University, 518060, China

DOI: 10.1109/JPHOT.2015.2505145

Manuscript received October 20, 2015; revised November 27, 2015; accepted November 30, 2015. Date of publication December 3, 2015; date of current version December 14, 2015. This work was supported in part by the National Natural Science Foundation of China under Grant 61475103 and Grant 11404218, by the Natural Science Foundation of SZU under Grant 00002701, by the Project of the Department of Education of Guangdong Province under Grant 2014KTSCX114, and by the National Hi-Tech Research and Development Program of China under Grant 2015AA020515. Corresponding author: P. Qiu (e-mail: pingqiu@szu.edu.cn).

Abstract: Deep-tissue multiphoton microscopy (MPM) enables noninvasive optical imaging into the deep regions of the tissue in animal models *in vivo*. High-order MPM techniques, such as three- and four-photon fluorescence microscopy at the 1700-nm window, are emerging as promising imaging techniques for deeper penetration. Currently, signal depletion at large imaging depth sets the depth limit for these imaging techniques. As a result, how to further boost signal level is the key to achieving a larger imaging depth. Contrary to the previous thought that overfilling the back aperture of the objective yields the highest multiphoton fluorescence signal, in this paper, through numerical simulation, we show that, due to the effect of exponential decay of the excitation beam, the signal generation is maximized for certain underfilling of the back aperture of the objective lens. This will provide a simple strategy for signal generation maximization in deep-tissue MPM and potentially enables deeper imaging penetration into the tissue.

Index Terms: Multiphoton microscopy, deep-tissue, three-photon, four-photon.

1. Introduction

Multiphoton fluorescence microscopy [1]–[3], combining subcellular resolution, 3-D sectioning, deep-tissue penetration in scattering biological tissue, label or genetic-modification based structure specificity, and functional imaging capability, enables scientists in various fields including neuroscience [4], [5], embryology [6], and oncology [7] to visualize *in vivo* and *ex vivo* tissue morphology and physiology. Multiphoton fluorescence microscopy involves excitation with n-photons ($n \geq 2$ and is an integer) simultaneously and emission of one fluorescence photon for

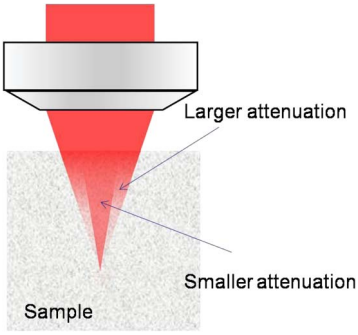

Fig. 1. Schematic of beam focusing into lossy samples. The rays at larger angles experience larger attenuation than those at smaller angles.

signal generation. 2-photon fluorescence microscopy (2PM) is the most commonly used imaging modality. However, for uniformly labeled tissue, imaging depth in mouse brain was limited to ~1 mm since the surface fluorescence overwhelmed the signal generated at the focus (signal-to-background ratio, or SBR reaches unity) [8]–[10]. Recently, 3-photon fluorescence microscopy (3PM) at the 1700-nm window was demonstrated to break this imaging depth limit [11]. This technique combines both reduction in attenuation of excitation at 1700 nm, compared with other wavelengths, and increase in SBR due to 3-photon excitation. As a result, we reached an imaging depth of 1.4 mm [12] in mouse brain in vivo, penetrating the white matter and imaging into the hippocampus in adult mouse [11]. Recently, at the same wavelength, we demonstrated that even higher order 4-photon fluorescence microscopy (4PM) [13] with higher SBR than with 3-photon could be achieved for in vivo deep-tissue imaging, extending the fluorophores coverage to the most commonly used GFP.

Both 3PM and 4PM promises a larger imaging depth than 2PM. Theoretically, 3PM at 1700 nm can image down to $> 9l_e$ (l_e: attenuation length of excitation beam due to both absorption and scattering) before SBR reaches unity [11] and larger can be expected for 4PM. However, currently the imaging depth is only limited to $< 4l_e$ for 3PM. This discrepancy is due to the depletion of the signal. There are two factors leading to the decay of the excitation beam and hence signal in tissue such as brain: absorption and scattering [11], [14]. As we image deeper, the excitation beam as well as signal decays exponentially. Finally, the signal is so weak that it is below the noise floor of the detection system. Apparently a boost in signal level will enable a larger imaging depth.

Here, we suggest a method for boosting signal level in 3PM and 4PM, by underfilling the back aperture of the high numerical aperture (NA) objective lens. The common deed in multiphoton fluorescence microscopy was to overfill the back aperture to maximize signal and to get the highest resolution [15]. For example, under scalar approximation, 3PM and 4PM signals are proportional to NA^2 and NA^4, respectively. This means overfilling the back aperture of the objective lens maximizes the signal. Underfilling leads to a decrease in the effective NA and signal reduction. However, we realize that in deep-tissue 3PM and 4PM, there is a competing effect that could lead to signal reduction as the back aperture became more filled: The rays converging at a larger angle will experience more attenuation than those at smaller angles (see Fig. 1). Consequently, for fixed power deposited on the sample after the objective lens, the more the lens filled, the smaller the signal due to the excessive loss experienced by the large-angle rays. In this paper, through numerical simulation of the vectorial electric field distribution around the focus of the high NA objective, we demonstrate that there exist optical filling factors which may be employed for boosting signal levels in deep-tissue 3PM and 4PM. To account for possible resolution reduction due to underfilling, we also present results of 3PM and 4PM point spread functions (PSFs) along the x, y, and z axes.

2. Simulation Details

Omitting irrelevant constants, 3PM and 4PM signals are given by

$$S_3 = \int I^3(\rho, \varphi, z)\mathrm{dV} \tag{1}$$

$$S_4 = \int I^4(\rho, \varphi, z)\mathrm{dV} \tag{2}$$

where S_3 and S_4 are the 3PM and 4PM signals, respectively; $I(\rho, \varphi, z) = |E(\rho, \varphi, z)|^2$ is the intensity in the cylindrical coordinates. After omitting a constant, the vectorial electric field distribution around the focus of the high NA objective lens is given by [16], [17]

$$\begin{bmatrix} E_x(\rho, \varphi, z) \\ E_y(\rho, \varphi, z) \\ E_z(\rho, \varphi, z) \end{bmatrix} = \begin{bmatrix} I_{00} + I_{02}\cos(2\varphi) \\ I_{02}\sin(2\varphi) \\ -i2I_{01}\cos\varphi \end{bmatrix} \tag{3}$$

$$I_{00} = \int_0^{\alpha_{\max}} E^{\mathrm{inc}}(\alpha)\sin\alpha\sqrt{\cos\alpha}(1+\cos\alpha)J_0(k\rho\sin\alpha)\exp(ikz\cos\alpha)d\alpha \tag{4}$$

$$I_{01} = \int_0^{\alpha_{\max}} E^{\mathrm{inc}}(\alpha)\sin^2\alpha\sqrt{\cos\alpha}J_1(k\rho\sin\alpha)\exp(ikz\cos\alpha)d\alpha \tag{5}$$

$$I_{02} = \int_0^{\alpha_{\max}} E^{\mathrm{inc}}(\alpha)\sin\alpha\sqrt{\cos\alpha}(1-\cos\alpha)J_2(k\rho\sin\alpha)\exp(ikz\cos\alpha)d\alpha. \tag{6}$$

In the above equations, $E^{\mathrm{inc}}(\alpha)$ is the angular distribution of the linearly polarized incident electrical field, k is the wave vector in water for water immersion objective lens, and $\alpha_{\max}$ is the maximum angle of integration.

In our simulation, we consider two types of incident fields, plane wave and Gaussian beam. For a reasonable comparison of signal levels, we keep the power after the objective lens the same for different filling factors. This allows us to maximize the signal for a fixed power on the sample. The scaled $E^{\mathrm{inc}}(\alpha)$ for plane wave and Gaussian beams, after angular-dependent attenuation are taken into account [17], [18] are given by

$$E^{\mathrm{inc}}_{\mathrm{plane}}(\alpha) = \frac{1}{\beta}\exp\left(-\frac{l_{\mathrm{depth}}}{2l_e\cos\alpha}\right) \tag{7}$$

$$E^{\mathrm{inc}}_{\mathrm{Gaussian}}(\alpha)\frac{1}{\beta}\sqrt{\frac{1-\exp(-2)}{1-\exp(-2/\beta^2)}}\exp\left(-\frac{\sin^2\alpha}{\beta^2\sin^2\alpha_{\max}}\right)\exp\left(-\frac{l_{\mathrm{depth}}}{2l_e\cos\alpha}\right) \tag{8}$$

where l_{depth} is the imaging depth, and β is the filling factor accounting for the extent to which the objective lens is filled. We note that β takes different values for plane wave and Gaussian beam incidence, i.e., $\beta \leq 1$ for plane wave while there is no such upper limit for Gaussian beam.

Similar to experiments, laser wavelength is 1700 nm for deep penetration, and the water immersion objective lens has a high NA of 1.05. The corresponding refractive index of water is 1.3145 at this wavelength. In our simulation, we calculated 3-photon and 4-photon signals using (1) and (2) to find out optimal filling factors β_{opt} for both plane wave and Gaussian beam incidence at different ratios of l_{depth}/l_e. The boundary of integration was chosen such that the corresponding intensity $I(\rho, \varphi, z)$ dropped to 1/10 of its maximum value at the focus (the drops of $I^3(\rho, \varphi, z)$ and $I^4(\rho, \varphi, z)$ were $1/10^3$ and $1/10^4$, respectively). 3PM and 4PM point spread functions (PSFs) measured at full-width-at-half-maximum of the signal along x, y, and z were also calculated for an estimation of resolutions.

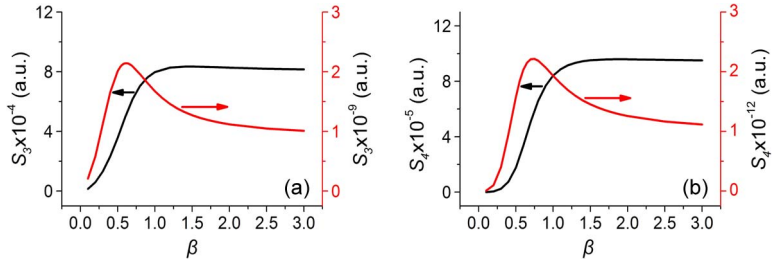

Fig. 2. 3-photon (a) and 4-photon (b) signals for various filling factors under plane wave illumination. Black curves: without attenuation; red curves: $l_{depth}/l_e = 3.82$.

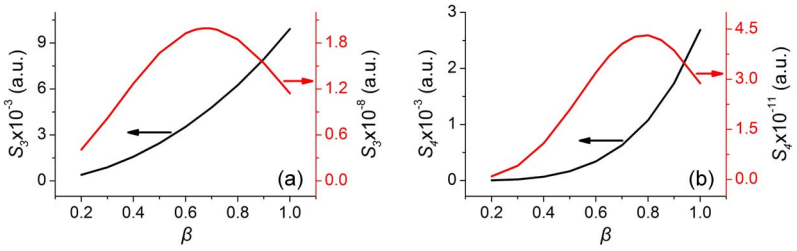

Fig. 3. 3-photon (a) and 4-photon (b) signals for various filling factors under plane Gaussian beam illumination. Black curves: without attenuation; red curves: $l_{depth}/l_e = 3.82$.

3. Simulation Results

3.1. Multiphoton Signal vs Filling Factors With and Without Attenuation

First, we illustrate the idea of optimal filling, by comparing the dependence of multiphoton signals on filling factors with attenuation and without attenuation. Fig. 2 shows that under plane wave illumination without attenuation of the excitation beam, both S_3 and S_4 (black curves) reach their maxima at largest filling of the back aperture $(\beta = 1)$, in agreement with previous analysis [15]. However, in the presence of attenuation, the peak S_3 and S_4 positions shift to smaller filling factors (see Fig. 2, red curves). Specifically, for $l_{depth}/l_e = 3.82$, the optimal filling factors β_{opt} for S_3 and S_4 are 0.68 and 0.79, respectively. The corresponding imaging depth l_{depth} for a measured $l_e = 365$ μm [11] is 1.4 mm. Compared with overfilling at $\beta = 1$, S_3 and S_4 are 1.7 and 1.5 times higher, respectively, justifying that underfilling the back aperture indeed boosts signal levels for both 3PM and 4PM. Extension of imaging depth Δz can be evaluated by $\exp(3\Delta z/l_e) = S(\beta = \beta_{opt})/S(\beta = 1)$ for 3PM, given that SBR > 1. For example, $\Delta z = 67.4$ μm for $l_e = 365$ μm and $l_{depth} = 1.4$ mm for 3PM. The larger $S(\beta = \beta_{opt})/S(\beta = 1)$, the larger Δz.

From an experimental perspective, the excitation beam sometimes can be well approximated by a Gaussian beam, especially when it is from a large-mode-area (LMA) fiber [19] or a photonic-crystal (PC) rod. Without attenuation, both S_3 and S_4 reach their maximum, then slightly drop and tend to a fixed value as β increases (see Fig. 3, black curves), since Gaussian beam illumination tends to plane wave illumination in the limit that $\beta \to \infty$. However, in the presence of attenuation $(l_{depth}/l_e = 3.82)$, there still exist optimal filling factors which maximize both S_3 and S_4 (see Fig. 3, red curves), similar to those for plane wave illumination. The corresponding optimal filling factors β_{opt} for S_3 and S_4 are 0.62 and 0.73, respectively.

From both Figs. 3 and 4, we find that the optimal filling factor for S_3 is smaller than that for S_4. This can be qualitatively explained by the nonlinear nature of signal generation in MPM. As we mentioned in the introduction, under scalar approximation, 3PM and 4PM signals are proportional to NA^2 and NA^4, respectively. This means a higher NA is favored for higher order

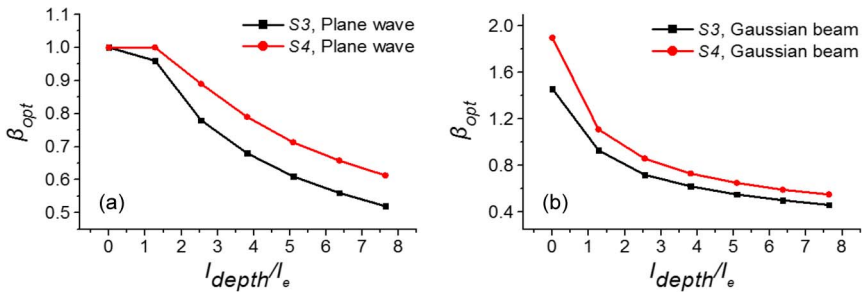

Fig. 4. Optimal filling factors for various *ratios of* l_{depth}/l_e under plane wave (a) and Gaussian beam (b) illumination.

MPM signal generation and leads to the relatively larger optimal filling factor for S_4 compared with S_3 in the presence of attenuation.

3.2. Optimal Filling Factors for Various Ratios of l_{depth}/l_e

Experimentally, either the imaging depth or the effective attenuation length may vary. To maximize MPM signals accounting for these variations, next through numerical simulation we investigate optimal filling factors for various ratios of l_{depth}/l_e. Fig. 4 shows that for both S_3 and S_4 under either plane wave or Gaussian beam illumination, as the ratio l_{depth}/l_e increases which leads to more attenuation of the large-angle rays, we need a smaller filling factor to avoid this excessive loss and to maximize signal. For example, for $l_{depth}/l_e = 7.63$ (corresponding to an imaging depth of $l_{depth} = 2.79$ mm for $l_e = 365$ μm), β_{opt} for S_3 under plane wave illumination is 0.52, and it is only half of that when there is no attenuation $(\beta = 1)$. Still, β_{opt} for S_4 is larger than that for S_3 for both illuminations. For example, for the same ratio of $l_{depth}/l_e = 7.63$ under plane wave illumination, β_{opt} for S_4 is 0.61. The calculated S_3 and S_4 under optimal filling conditions are 4.66 and 4.51 times higher than those under overfilling conditions $(\beta = 1)$.

3.3. Spatial Resolutions

According to the results given above, underfilling the back aperture in the presence of attenuation indeed helps boosting MPM signals. However, it can be expected this will lead to deterioration of spatial resolutions. Fig. 5 shows variation of PSFs along the three axes for various attenuations under plane wave illumination. The black curves in Fig. 5 were calculated PSFs corresponding to optimal filling factors shown in Fig. 4(a). For comparison, PSFs corresponding to overfilling $(\beta = 1)$ were also calculated (red curves in Fig. 5). Fig. 5 clearly shows that 3-photon and 4-photon signal maximization through optimal filling comes at the cost of resolution reduction along all axes. For example, at $l_{depth}/l_e = 3.82$, 3-photon PSFx, PSFy, and PSFz are increased by 27.5%, 39.7%, and 129%, respectively. 4-photon PSFx, PSFy, and PSFz are increased by 13.9%, 21.6%, and 65.9%, respectively. PSF deterioration for 3-photon is worse than for 4-photon, since β_{opt}s for 3-photon are smaller than for 4-photon (see Fig. 4). For both 3-photon and 4-photon, PSFz suffer more from underfilling than PSFx and PSFy. As attenuation (l_{depth}/l_e) increases, PSFs deteriorate even more as more underfilling is required and β_{opt} becomes smaller (see Fig. 4). Deterioration in PSFs is also observed for Gaussian beam illumination (see Fig. 6).

3.4. Impact on SBR

Intuitively, the smaller the filling factor, the more background fluorescence will be generated near the surface of the sample, leading to a decrease in SBR. As we mentioned before, SBR > 1 is the prerequisite for multiphoton fluorescence microscopy. Next, we evaluate SBR under optimal filling condition for 3-photon excitation and plane wave illumination. Background fluorescence calculation is in accordance with our previous theoretical analysis [11], assuming

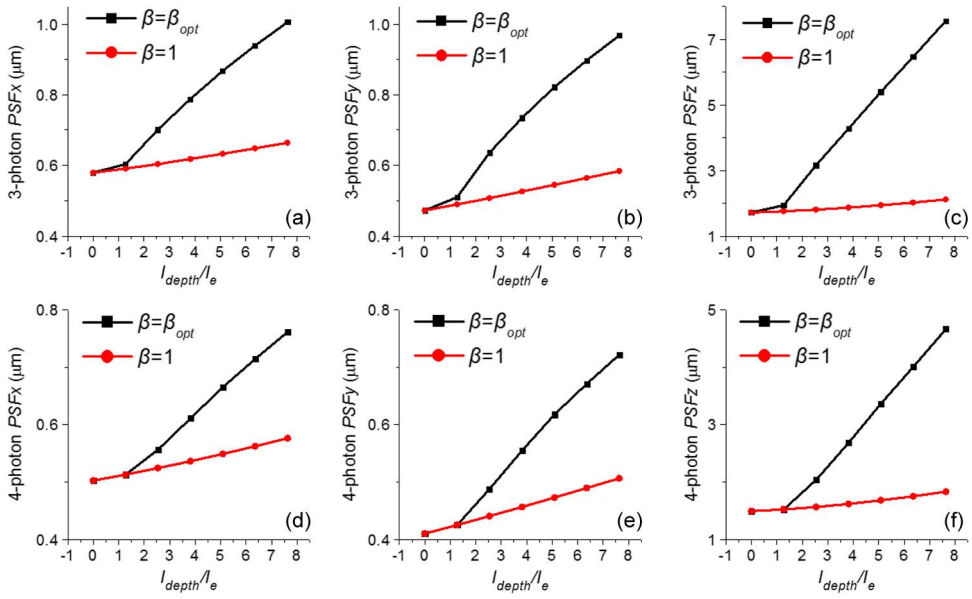

Fig. 5. Calculated PSFs vs I_{depth}/I_e for 3-photon (a)–(c) and 4-photon (d)–(f) under plane wave illumination. Black curves: PSFs corresponding to optimal filling; red curves: PSFs corresponding to overfilling $\beta = 1$.

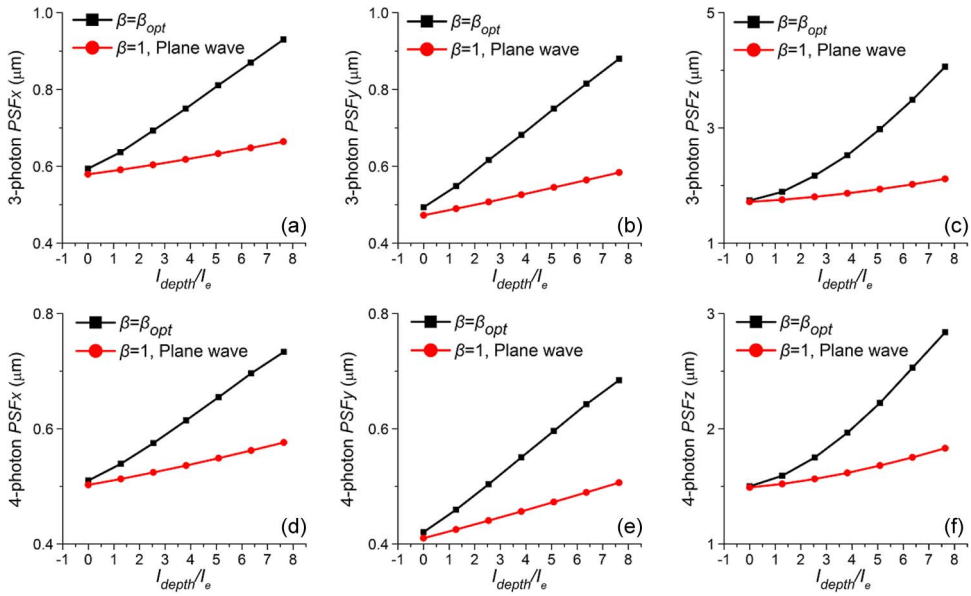

Fig. 6. Calculated PSFs vs I_{depth}/I_e for 3-photon (a)–(c) and 4-photon (d)–(f). Black curves: PSFs corresponding to optimal filling under Gaussian beam illumination; red curves: PSFs corresponding to overfilling $\beta = 1$ under plane wave illumination.

the background is generated mainly within one effective attenuation length of the sample surface. Then, SBR is

$$\text{SBR} = \frac{\beta^4}{\pi\left(\frac{I_{\text{depth}}\text{NA}^2}{I_e\sqrt{n^2-\beta^2\text{NA}^2}}\right)^2 I_e^3}\int I^3(\rho,\varphi,z)\text{dV} \tag{9}$$

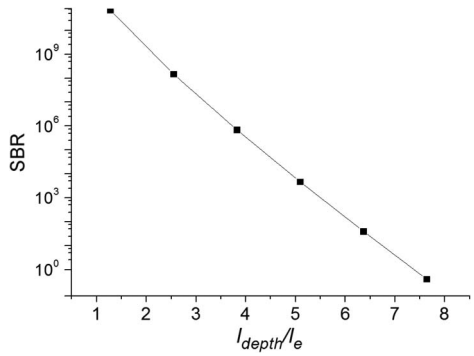

Fig. 7. Calculated SBRs vs l_{depth}/l_e for 3-photon under plane wave illumination and optimal filling. $l_e = 365$ μm, and $f = 4.5$ mm.

where n is the refractive index of water, and f is the focal length of the objective lens. The constant $ikf\exp(-ikf)/2$ originally omitted in (3) was taken into account in deriving (9), and f is the focal length of the objective lens. Fig. 7 shows calculated 3-photon SBR results corresponding to various l_{depth}/l_e at optimal filling. For the largest ratio of $l_{depth}/l_e = 7.63$ we considered, SBR drops to 0.41, which is 22% smaller than that under overfilling (SBR $= 0.52$ for $\beta = 1$). For this specific case, optimal filling still enables 3-photon imaging down to a depth of $\sim 7.4 l_e$.

4. Conclusion and Discussion

To maximize signal generation for high-order, deep-tissue multiphoton fluorescence microscopy, in this paper, we suggested underfilling the back aperture of the high-NA objective lens. Through numerical simulation we demonstrated that, there was an optimal filling factor for each ratio of l_{depth}/l_e. As this ratio increases, corresponding to an increase in imaging depth or attenuation, β_{opt} becomes smaller to avoid excessive loss of excitation light due to the large-angle rays. Experimentally, variable beam expanders (with tunable expansions) can be used to continuously change the filling factors. Admittedly, compared with overfilling, this method comes at the expense of deterioration of spatial resolutions manifested by the calculated PSFs along all the three axes. Therefore, there is a comprise between maximizing the MPM signal generation and sacrificing spatial resolution using the proposed method. However, for deep-tissue MPM, sometimes the first goal is to be able to see the structures, for example, neurons in deep layers of the brain. From this perspective, sacrifice in spatial resolution may be acceptable, given that maximizing signals allows a larger imaging depth. We also note that the optimal filling method suggested in this paper doesn't mean that a small-NA objective should be chosen for deep-tissue MPM, since a high-NA objective lens collects more fluorescence, which is required. Therefore, a high-NA objective should be chosen but optimally underfilled to maximize MPM signal generation.

Acknowledgment

The authors are much obliged to Prof. C. Xu from Cornell University for the inspiring discussion of this work.

References

[1] W. Denk, J. H. Strickler, and W. W. Webb, "Two-photon laser scanning fluorescence microscopy," *Science*, vol. 248, no. 4951, pp. 73–76, Apr. 1990.
[2] S. W. Hell *et al.,* "Three-photon excitation in fluorescence microscopy," *J. Biomed. Opt.*, vol. 1, no. 1, pp. 71–74, Jan. 1996.
[3] S. Maiti, J. B. Shear, R. Williams, W. Zipfel, and W. W. Webb, "Measuring serotonin distribution in live cells with three-photon excitation," *Science*, vol. 275, no. 5299, pp. 530–532 Jan. 1997.
[4] J. N. Kerr and W. Denk, "Imaging in vivo: Watching the brain in action," *Nat. Rev. Neurosci.*, vol. 9, no. 3, pp. 195–205, Mar. 2008.

[5] D. A. Dombeck, C. D. Harvey, L. Tian, L. L. Looger, and D. W. Tank, "Functional imaging of hippocampal place cells at cellular resolution during virtual navigation," *Nat. Neurosci.*, vol. 13, no. 11, pp. 1433–1440, Nov. 2010.
[6] N. Olivier *et al.,* "Cell lineage reconstruction of early zebrafish embryos using label-free nonlinear microscopy," *Science*, vol. 329, no. 5994, pp. 967–971, Aug. 2010.
[7] R. M. Williams *et al.,* "Strategies for high resolution imaging of epithelial ovarian cancer by laparoscopic nonlinear microscopy," *Transl. Oncol.*, vol. 3, no. 3, pp. 181–194, Jun. 2010.
[8] P. Theer, M. T. Hasan, and W. Denk, "Two-photon imaging to a depth of 1000 μm in living brains by use of a Ti:Al2O3 regenerative amplifier," *Opt. Lett.*, vol. 28, no. 12, pp. 1022–1024, Jun. 2003.
[9] D. Kobat *et al.,* "Deep tissue multiphoton microscopy using longer wavelength excitation," *Opt. Exp.*, vol. 17, no. 16, pp. 13 354–13 364, Aug. 2009.
[10] R. Kawakami *et al.,* "Visualizing hippocampal neurons with in vivo two-photon microscopy using a 1030 nm pico-second pulse laser," *Sci. Rep.*, vol. 3, no. 1014, pp. 1–7, 2013.
[11] N. G. Horton *et al.,* "In vivo three-photon microscopy of subcortical structures within an intact mouse brain," *Nat. Photon.*, vol. 7, no. 3, pp. 205–209, 2013.
[12] N. G. Horton, K. Wang, C.-C. Wang, and C. Xu, "In vivo three-photon imaging of subcortical structures of an intact mouse brain using quantum dots," in *Proc. IEEE CLEO EUROPE/IQEC Conf.*, 2013, p. 1.
[13] L.-C. Cheng, N. G. Horton, K. Wang, S.-J. Chen, and C. Xu, "Measurements of multiphoton action cross sections for multiphoton microscopy," *Biomed. Opt. Exp.*, vol. 5, no. 10, pp. 3427–3433, Oct. 2014.
[14] K. Wang, N. Horton, K. Charan, and C. Xu, "Advanced fiber soliton sources for nonlinear deep tissue imaging in biophotonics," *IEEE. J. Sel. Topics Quantum Electron.*, vol. 20, no. 2, Mar./Apr. 2013, Art. ID 6800311.
[15] C. Xu and W. Webb, "Multiphoton Excitation of Molecular Fluorophores and Nonlinear Laser Microscopy," in *Topics in Fluorescence Spectroscopy*, vol. 5. New York, NY, USA: Springer-Verlag, 2002, pp. 471–540.
[16] J.-X. Cheng, A. Volkmer, and X. S. Xie, "Theoretical and experimental characterization of coherent anti-Stokes Raman scattering microscopy," *J. Opt. Soc. Amer. B*, vol. 19, no. 6, pp. 1363–1375, 2002.
[17] L. Novotny and B. Hecht, *Principles of Nano-Optics*. Cambridge, U.K.: Cambridge Univ. Press, 2012.
[18] P. Theer and W. Denk, "On the fundamental imaging-depth limit in two-photon microscopy," *J. Opt. Soc. Amer. A*, vol. 23, no. 12, pp. 3139–3149, Dec. 2006.
[19] K. Wang and C. Xu, "Tunable high-energy soliton pulse generation from a large-mode-area fiber and its application to third harmonic generation microscopy," *Appl. Phys. Lett.*, vol. 99, no. 7, 2011, Art. ID 071112.